10.3.2 Results

In Fig. 10.26 the distributions of temperature and pore water pressure at three points in time are depicted. 13 days after the heating has been initiated ($t = 45\,\mathrm{d}$), a zone of increased pore pressure can be observed. This is caused by the thermal expansion of the fluid in a low permeable medium.

Results of three different numerical codes are presented in Fig. 10.27. ANSYS [4] and FLAC3D [5] are applied besides OGS. The temporal evolutions of the main variables are shown at four points along the x-axis. Only minor derivations can be observed, which are explainable by differences in the discretization and the modeling approach. For instance, advective heat transport is considered by OGS only.

10.4 Consolidation Under Two-Phase Flow Condition: Five Spot Example

Wenqing Wang

Wang, W. (2015) " Consolidation Under Two-Phase Flow Condition: Five Spot Example, in Thermo-Hydro-MechanicalChemical Processes in Fractured Porous Media: Modelling and Benchmarking Closed-Form Solutions, Edited by Kolditz et al., Springer "

The example is based on a classic two-phase flow example for benchmark purpose [6], which describes a sort of water flooding process in porous media, and it is expended hereby with an elastic deformation.

Assuming that the density of the each phase is constant, the process can be described by the mass balance equations and the momentum balance equation. With the capillary pressure p^c and the non-wetting phase pressure p^{nw} as two primary variables, the mass balance equations are given as

$$n\rho^w \frac{\partial S^w}{\partial p^c}\frac{\partial p^c}{\partial t} - \nabla\cdot\left[\rho^w \frac{\mathbf{k}k^w_{rel}}{\mu^w}\left(\nabla(p^{nw}-p^c)-\rho^w\mathbf{g}\right)\right] + S^w\rho^w\frac{\partial}{\partial t}\nabla\cdot\mathbf{u} = Q_w \tag{10.3}$$

$$-n\rho^{nw}\frac{\partial S^w}{\partial p^c}\frac{\partial p^c}{\partial t} + (1-S^w)n\left(\frac{\partial \rho^{nw}}{\partial p^{nw}}\frac{\partial p^{nw}}{\partial t} + \frac{\partial \rho^{nw}}{\partial p^c}\frac{\partial p^c}{\partial t}\right) - \nabla\cdot\left[\rho^{nw}\frac{\mathbf{k}k^{nw}_{rel}}{\mu^{nw}}\left(\nabla p^{nw}-\rho^{nw}\mathbf{g}\right)\right] + (1-S^w)\rho^{nw}\frac{\partial}{\partial t}\nabla\cdot\mathbf{u} = Q_{nw} \tag{10.4}$$

where nw indicates the non-wetting phase, w indicates the wetting phase, S is saturation, $\mathbf{u}$ is the displacement, n is the porosity, ρ denotes the density, Q denotes the source/sink term, $\mathbf{k}$ is the intrinsic permeability, k^w_{rel} and k^{nw}_{rel} represents the relative permeability of phases, μ denotes the viscosity, and $\mathbf{g}$ is the vector of gravity.

While, the momentum balance equation takes the following form

$$\nabla\cdot\left(\boldsymbol{\sigma} - (p^{nw} - S^w p^c)\,\mathbf{I}\right) + \rho\mathbf{g} = 0 \tag{10.5}$$

where $\boldsymbol{\sigma}$ is the effective stress of the porous medium, and $\mathbf{I}$ is the identity tensor. The density of the porous medium is composed by three phases, two fluids and solids $\rho = nS^w\rho^w + n(1-S^w)\rho^{nw} + (1-n)\rho^s$ with ρ^s, the solid density. The unknowns of the momentum equation is the displacement, $\mathbf{u}$, and which is solved via the constitutive law

$$\boldsymbol{\sigma} = \mathbb{C}\boldsymbol{\epsilon}$$

and the strain displacement relationship

$$\boldsymbol{\epsilon} = \left((\nabla\mathbf{u})^T + \nabla\mathbf{u}\right)/2$$

where $\mathbb{C}$ is the stress strain tensor, and the subscript T means transpose.

Due to the symmetry, we take one quarter of the five spot example with a size of $10 \times 10 \times 1\,\mathrm{m}^3$. The fluids that are assumed to be involved in the process are water (wetting phase) and hydrocarbon (non-wetting phase). The material parameters are given in Table 10.8. In the original definition of the problem, the capillary pressure is small and omitted. Since the capillary pressure is adopted as one of the primary variables in the present mass balance equations, we employ the van Genuchten model as

$$p^c = \frac{\rho^w \mathrm{g}}{\alpha}\left[S_{\mathrm{eff}}^{-1/m_v} - 1\right]^{1/n_v} \tag{10.6}$$

where α [1/m] is a conceptualized parameter related to the air entry pressure, n_v is a dimensionless pore size distribution index and $m_v = 1 - (1/n_v)$, and S_{eff} is the effective saturation defined as

$$S_{\mathrm{eff}} = \frac{S^w - S_r^w}{S_{\max}^w - S_r^w} \tag{10.7}$$

with $S_{\max}^w$ and S_r^w as the maximum and residual saturation. In this example, we set $m_v = 0.7$, $S_{\max}^w = 1$, $S_r^w = 0$, and $\alpha = 0.37$.

Table 10.8 Material properties of five-spot example

Property	Value	Unit
Water density	1000	$\mathrm{kg/m}^3$
Hydocarbons density	1000	$\mathrm{kg/m}^3$
Water viscosity	10^{-3}	Pa s
Hydocarbons viscosity	4×10^{-3}	Pa s
Porosity	0.206	–
Intrinsic permeability	10^{-13}	m^2
Relative permeability	$k_{rel}^w = (S^w)^2$, $k_{rel}^{nw} = (1-S^w)^2$	–
Capillary-saturation relationship	van Genuchten	Pa
Young's modulus	3.5×10^{10}	Pa
Poisson ratio	0.3	–

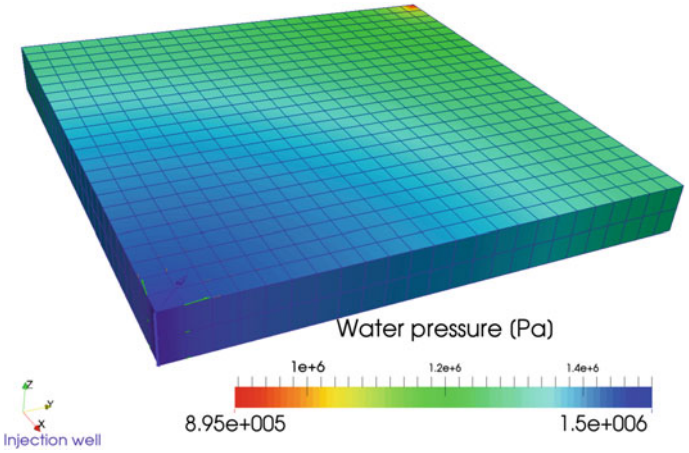

Fig. 10.28 Mesh and water pressure distribution after 20 days

Initially, the capillary pressure is set to $p_0^c = 105018\,\text{Pa}$ to represent a very small water saturation of 0.04, meanwhile the non-wetting phase pressure is given as $p_0^{nw} = p_0^c\,\text{Pa}$ to represent that there is no water pressure at the beginning of the injection/pumping. Besides, the initial effective stresses are all zero by omitting the gradational force.

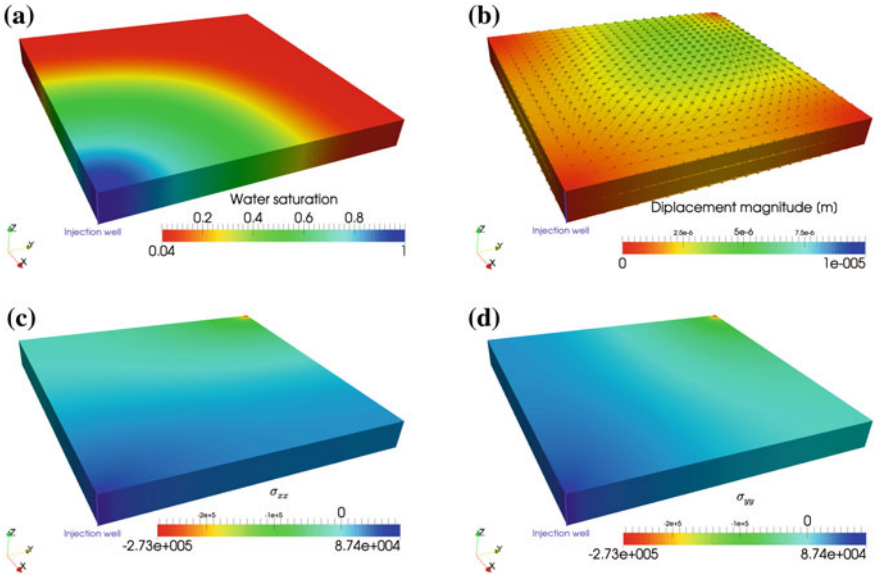

Fig. 10.29 Variable distribution after 20 days' injection. **a** Water saturation, **b** Displacement magnitude, **c** Effective stress σ_{xx}, **d** Effective stress σ_{yy}

At the injection corner, the boundary conditions are prescribed as $p^c = 0$ and 1.5×10^6 Pa, while at the pumping corner, the non-wetting phase pressure is 10^6 Pa. The displacement in the normal direction of all surface is restricted to zero. The time duration of the pumping is 20 days.

The domain is discretized into 1,151 hexahedral elements with 1,875 nodes, which is demonstrated in Fig. 10.28. Figure 10.28 also shows the calculated water pressure (calculated by $p^{nw} - p^w$) distribution at 20 days.

After 20 days' injection, the distribution of other variables is shown in Fig. 10.29a, b, c and d respectively. Figure 10.29 prompts that there is tensile effective stresses increasing in the vicinity of the injection well. Since there is not any mechanical load applied to the domain, the changes of the effective stresses are caused by the changes of fluid pressures solely. We can see this hydraulic mechanical coupling more distinctively with the following variable profiles (Fig. 10.30), which are plotted along one horizontal edge of the domain that starts from the injection well.

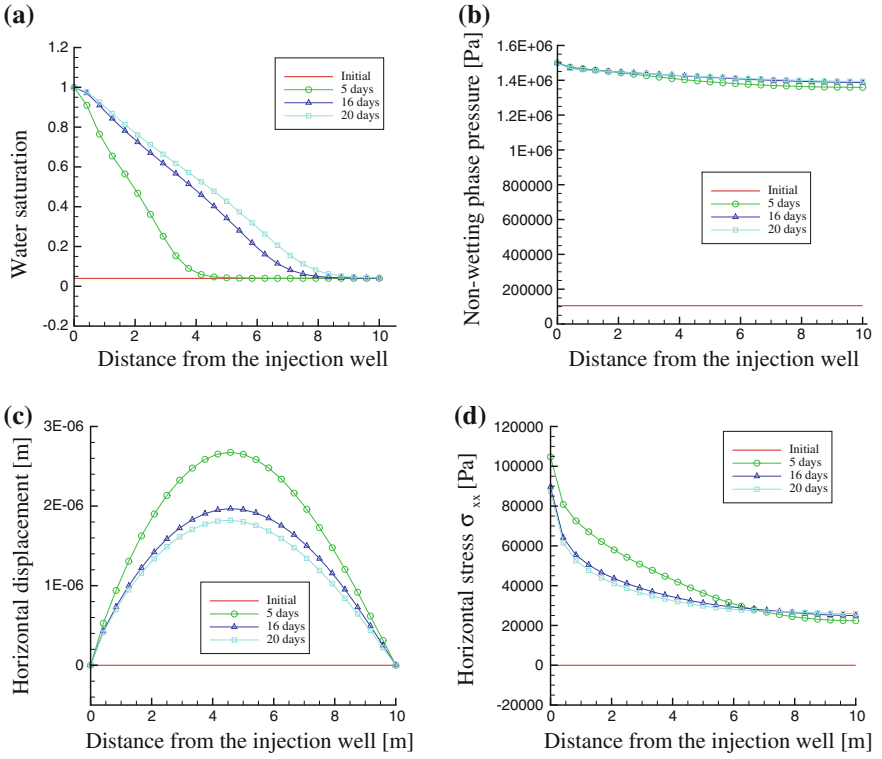

Fig. 10.30 Profiles along one horizontal edge that starts from the injection well. **a** Water saturation, **b** Non-wetting phase pressure, **c** Horizontal displacement, **d** Effective stress σ_{xx}

References

1. Abaqus. Abaqus FEA. Technical report, Dassault Systémes, 2007.
2. J. C. Jaeger, N. G. W. Cook, and R. W. Zimmerman. *Fundamentals of Rock Mechanics (4th Edition)*. John Wiley & Sons, 2007.
3. M. Jobmann. Methodik und Anwendungsbezug eines Sicherheits- und Nachweiskonzeptes für ein HAW-Endlager im Tonstein, ANSICHT. Jahresbericht 2012, DBE-Tec, 2013.
4. ANSYS Inc., Minnesota, USA. *ANSYS Mechanical, Help System, Mechanical APDL Documentation*. Release 14.5.7.
5. ITASCA Consultants, Minnesota, USA. *FLAC3D Manuals*, 3.1 edition, 2006.
6. K. Aziz and A. Settari. *Petroleum reservoir simulation*, volume 476. Applied Science Publishers London, 1979.